



Enhancing the Strain Sensitivity of Carbon Nanotube-Polymer Thin Films For Damage Detection and Structural Monitoring

Y. Zhao^{1,5}, C. Viechtbauer^{2,5}, K.J. Loh³, M. Schagerl^{4,5}

- 1 Research Fellow, Institute of Constructional Lightweight Design, Johannes Kepler University Linz, Austria.
E-mail: yingjun.zhao@jku.at (corresponding author)
- 2 Research Associate, Institute of Constructional Lightweight Design, Johannes Kepler University Linz, Austria.
E-mail: christoph.viechtbauer@jku.at
- 3 Associate Professor, Dept. of Civil & Environmental Engineering, University of California, Davis, United States.
E-mail: kjloh@ucdavis.edu
- 4 Professor, Institute of Constructional Lightweight Design, Johannes Kepler University Linz, Austria.
E-mail: martin.schagerl@jku.at
- 5 Christian Doppler Laboratory for Structural Strength Control of Lightweight Constructions, Linz, Austria.

ABSTRACT

Today the rapid growth of fiber-reinforced polymer (FRP) applications in the automotive and aerospace industry has motivated many researches to perform life-cycle analyses of FRP structures. While its strength-to-weight ratio outperforms conventional metals, FRP is inherently heterogeneous and experiences complex failure modes, thus making them challenging for structural analysis and design. Assessing structural conditions such as employing structural health monitoring (SHM) sensors to observe its *in-situ* behavior may help prevent large-scale structural failure while simultaneously providing a chronological account of structural behavior due to known damage occurrences. Among the various SHM techniques, carbon nanotube (CNT)-polymer thin films can be rapidly applied onto FRP surfaces, or possibly embedded in the material, for damage detection. In this study, the strain sensitivity of embedded CNT-polymer thin film strain sensors was improved by nearly three times. The goal was to use these sensors to capture mild structural deformation by measuring induced strains in the structure. Furthermore, the geometrical influence of a thin film on its electrical response was investigated. Both results provided guidance as to how these sensors could be eventually applied for real-world FRP structures.

KEYWORDS: carbon nanotubes, nanocomposite, electromechanical, strain sensing, structural monitoring

1. INTRODUCTION

Employing fiber-reinforced polymer (FRP) composites to construct load-bearing structural components currently proliferates in the automotive [1, 2], aerospace [3, 4], civil [5], and biomedical [6] industries. Carbon fiber-reinforced polymers (CFRP) are particularly favored by lightweight-designed structures. BMW i3 and i8, which are recently-launched electrical/hybrid vehicles developed by BMW Group, adopt CFRPs for their passenger compartments in compensation for the weight of their Lithium-ion batteries [2]. Airbus and Boeing also launched FRP-dominated commercial aircraft whose fuselage, spoiler, and/or wings are composed by CFRPs (*e.g.*, the A350 series and the 787 Dreamliner) for improving their fuel efficiency [3, 4]. While it is advocated by the industry for its ultimate strength-to-weight ratio and resistibility to chemical corrosion, FRP suffers from a complex failure mode due to various reasons, such as its multivariate composition and inevitable inclusion of manufacturing flaws. Challenges are therefore posted to perform an FRP structure's life-cycle analysis due to lack of a complete understanding of its damage-to-failure mechanism. To learn more about the impact of damage upon an FRP structure's performance, a reliable, *in-situ* structural health monitoring (SHM) system is required.

Many nondestructive testing (NDT) methods for identifying structural damage are found to be applicable for FRP composites, such as acoustic emissions [7], ultrasonic C-scanning [8], and X-ray scanning [9]. Examples of NDT methods for metallic structures include passive acoustic sensors collecting vibrational signals from rotational machineries to identify their stiffness degradation or air-coupled ultrasonic waves propagating through a structure to identify minor through-thickness defects of metallic plates. Radiography can also capture minor variations in plate thickness caused by defects or damages. In addition to their applications for metals, these techniques have demonstrated their ability to locate, quantify, and/or qualify damage occurring within or on the surface of FRP composites. Foil-type strain gages and fiber-optic sensors are also useful for measuring local strain magnitude [10]. These sensors, however, either have to be accompanied with a strictly controlled

testing environment, which could be expensive to offer, or have to compromise between hardware cost and measurement resolution. Some of them may even interfere with a structure's conventional operation or deteriorate its intrinsic material strength [11]. To overcome these challenges, many researches are motivated to develop broad range monitoring sensors that are low-cost, lightweight, and easy to install with no trade-off of reliability or durability. Some of the research takes advantage of material assembling techniques offered by nanotechnology, and carbon nanotube-embedded materials are one of these emerging technologies showing great potential for SHM [12].

Carbon nanotube (CNT)-embedded polymeric composites can be assembled through various fabrication techniques; their applications as sensing materials include detection of strain, pressure, and presence of oxygen [13-17]. Possessing remarkable mechanical and electrical properties, CNT-integrated polymer composites can be casted into thin sheets that are particularly sensitive to, *e.g.*, strain. Lipomi *et al.* [13] spin-coated CNT-based poly(dimethylsiloxane) (PDMS) to form transparent, highly stretchable thin films that response to strain deformation in terms of change in material's resistance and capacitance. Park *et al.* [15] suspended multi-walled carbon nanotubes in polyethylene oxide (PEO) solution to fabricate nanocomposite thin film strips in similar geometry to strain gages; their resistance variations correlated both linearly and nonlinearly to applied strain. Loh *et al.* [18] fabricated piezoresistive CNT-polyelectrolyte thin films via the layer-by-layer (LbL) method, and the corresponding strain sensitivity or gage factor was ~ 6.5 , nearly three times higher than that of typical foil-type strain gages. When combined with an electrical impedance tomography (EIT) algorithm, similar thin films had been demonstrated for spatial damage detection in metallic coupons, lab-scale concrete beams, and composite coupons [18-21].

Despite these aforementioned advances, there still remain several technical challenges for applying this sensor technology to real structural components, primarily due to scalability and the size of sensors required. First, the thin film fabrication procedure needs to be simplified for large-scale, complex-shaped surfaces. Loyola *et al.* [22] and Mortenson *et al.* [17] developed a rapid assembly method to spray CNT-based thin film with an airbrush. A CNT-suspended polymeric ink can be sprayed like paint directly upon the target surface. Unlike other methods, thin films sprayed through this method may conform to any geometrical surfaces, and the fabrication time required is drastically reduced [19]. Although the as-fabricated thin film is capable of identifying severity and locations of impact damage [19], its low strain sensitivity is insufficient for capturing mild deformations.

In the first part of this paper, Pluronic will replace polystyrene sulfonates (PSS) in the original CNT ink formula for dispersing CNTs. Pluronic is a trademarked triblock copolymer exhibiting amphiphilic behavior, which makes it an excellent stabilizing agent for nanomaterials in aqueous solutions [23, 24]. Compared to PSS, Pluronic is able to create a more stable CNT suspension that lasts weeks or even longer. In this study, both CNT-PSS and CNT-Pluronic thin films will be sprayed onto polyamide coupons, and their strain sensitivities will be characterized using tensile cyclic tests. The second part of this paper intends to investigate the influence of a thin film's width to its gage resistance response, so as to verify its electrical behavior as the size of the film grows. Due to the material's piezoresistive nature, a change of its electrical property (*i.e.*, resistance) can be correlated to a strain deformation/damage along its gage length; as the width of the sensing area expands, it is unknown if a remote deformation in the transverse direction to the current path can affect the electrical signal significantly. In this test, a two-point probe resistance measurement was established on a rectangular-shaped CNT-PSS thin film. The same measurement was repeated after every reduction of the thin film's width. Results presented in this paper characterized the electromechanical behavior of CNT-embedded thin films, and better understanding of these films can facilitate their adoption as strain/damage sensors for practical FRP structures.

2. EXPERIMENTAL DETAILS

2.1. Electromechanical Characterization of CNT-Pluronic Thin Films

Two kinds of polymers in this study were used to create CNT-suspensions, namely poly(sodium 4-styrenesulfonate) (PSS) and Pluronic® F-127 (Pluronic). Together with multi-walled carbon nanotubes (MWNT), they were all purchased from Sigma-Aldrich. Details of the fabrication procedure of MWNT-PSS thin films can be found in Mortenson *et al.* [17] and Loyola *et al.* [22], whereas the fabrication details for the MWNT-Pluronic thin film will be discussed in the following section.

2.1.1. Thin film fabrication

The MWNT-suspended Pluronic solution was made in a similar fashion as that of the MWNT-PSS solution described by Mortenson *et al.* [17]. Pluronic powder was dissolved in deionized water to make a 2 wt.%

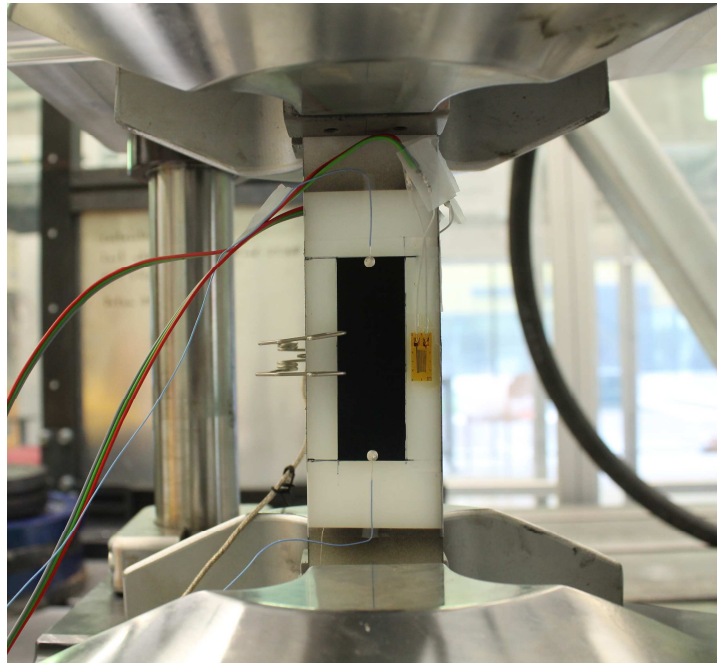


Figure 2.1 A PA 6 coupon with an MWNT-based film was mounted in the load frame for testing.

Pluronic solution. The mixture was heated at 50°C and constantly stirred on a hotplate until it became clear with no visible signs of the polymer. MWNTs were then mixed with the Pluronic solution, and a small amount of N-methyl-2-pyrrolidinone (NMP) was added to improve its adhesion to poly(vinylidene fluoride) (PVDF) or latex micro-particles, which was added in a following step. The mixture was then subjected to a 0.5 s-on, 0.5 s-off tip sonication for 60 min (Bandelin Sonopuls GM 70, 70 W, 20 kHz). The sonicated solution exhibits nearly homogenous properties similar to that of the MWNT-PSS solution [17]. Due to Pluronic's extraordinary stabilizing ability, the shelf life of the mixture could be weeks or even months without noticeable precipitation of MWNTs.

In order to bond the thin film tightly to its spraying surface, a PVDF latex micro-particle solution was added to the sonicated mixture as a binder. Moreover, it helps thicken the solution to facilitate spraying. A Kynar Aquatec ARC (a gift received from Arkema Inc.) latex solution was directly mixed with the CNT-Pluronic solution and sloshed to form a paint-like mixture. The added amount of PVDF shall be maintained at a level where the MWNT content of the final solid material is 5 wt.%. The spraying paint was then loaded into an airbrush (Agora-Tec, 0.5 mm tip) and sprayed over the polyamide 6 (PA 6) coupon surface. An infrared lamp (Philips IR 250 RH, 250 W) was hung over the coupon while spraying, so as to maintain the coupon's surface temperature to be approximately 55°C. This was performed to quickly coagulate the MWNT-Pluronic-PVDF paint as it bonds to the surface, since aqueous Pluronic thickens rapidly under elevated temperature and/or scarce humidity [25]. The sprayed thin films were left to air dry for at least 1 h. In this study a 60 mm × 20 mm thin film was painted over the midsection of a PA 6 tensile testing coupon as demonstrated in Figure 2.1, and five specimens for each type of thin film were prepared for testing.

2.1.2. Electromechanical test setup

The sprayed PA 6 coupons were 180 mm × 40 mm in dimension and subjected to cyclic tensile tests. As demonstrated in Figure 2.1, a PA 6 coupon was clamped onto an MTS 647 hydraulic wedge grip with an initial grip separation distance of 135 mm. A foil-type strain gage was attached to the mid-span of the coupon next to the CNT thin film, and an extensometer (MTS 634 31F-24) was installed on the back of the coupon. An HBM QuantumX MX840B multichannel data acquisition system was used to collect the thin film's two-point probe resistance measurements, as well as signals from the strain gage and the extensometer at a sampling rate of 100 Hz. Each coupon was loaded four times using a linear load-unload (triangular) tensile load pattern, where the peak load was 0.8 kN for the first two runs and 1.6 kN for the last two runs. A total set of 10 coupons were tested, with five of them sprayed with the MWNT-PSS thin films and the rest with MWNT-Pluronic thin films.

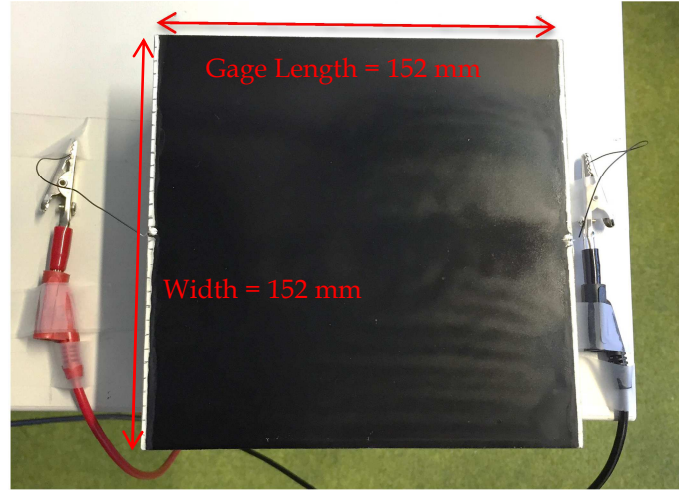


Figure 2.2 An MWNT-PSS thin film was sprayed over a G10-FR4 plate. Two wires were attached as demonstrated for measuring its gage resistance response with respect to width change (starting with 152 mm).

2.2. Dimensional Influence over Thin Film's Electrical Response

The goal of this test was to characterize how the fabricated thin film's width impacts its gage resistance response. Following the fabrication procedure discussed in Mortenson *et al.* [17], an MWNT-PSS thin film was sprayed over a 152 mm × 152 mm flame-retardant multipurpose garolite (G10-FR4) composite plate, as seen in Figure 2.2. A wire was attached at the midpoint of an edge using two-part silver epoxy, and a second wire was attached at the midpoint of the opposite edge. These wires are for obtaining the thin film's two-point probe resistance measurements along its gage length using an HP 34401A digital multimeter. The thin film's width was reduced by cutting off a 5-mm strip along one side of the thin film's gage length and the next on the other side. A resistance value was read after every width reduction. When the thin film's width, W , reached 7 mm, the step size was reduced to 1 mm until W became 1 mm.

3. RESULTS AND DISCUSSIONS

3.1. Electromechanical Characterization of CNT-Pluronic Thin Films

It should be firstly noticed that the displacement data from the extensometer and the strain gage were compared to check if possible bending could have occurred to the tensile coupons during loading. In addition, tensile strains calculated from extensometer's displacement data suggested that each coupon was slightly bent while loaded (*e.g.*, strain values calculated from the extensometer data were always higher than that of the strain gage on the opposite side of the coupon), with a strain difference of approximately 100-200 $\mu\text{m/m}$ between the opposite sides. Since the degree of bending was relatively minor and considerably irrelevant to the topic covered in this study, the result was omitted from this discussion.

The electromechanical response of the fabricated thin film was characterized by its normalized resistivity change, ρ_n , with respect to its strain, ϵ , due to deformation. A thin film's average resistivity was calculated as its resistance value normalized by its dimensions:

$$\rho = \frac{RA}{L} \quad (3.1)$$

where A is the cross-sectional area of the thin film, L is the gage length, and R is the measured resistance across L . The normalized resistivity change was therefore calculated as:

$$\rho_n = \frac{\rho - \rho_0}{\rho_0} \quad (3.2)$$

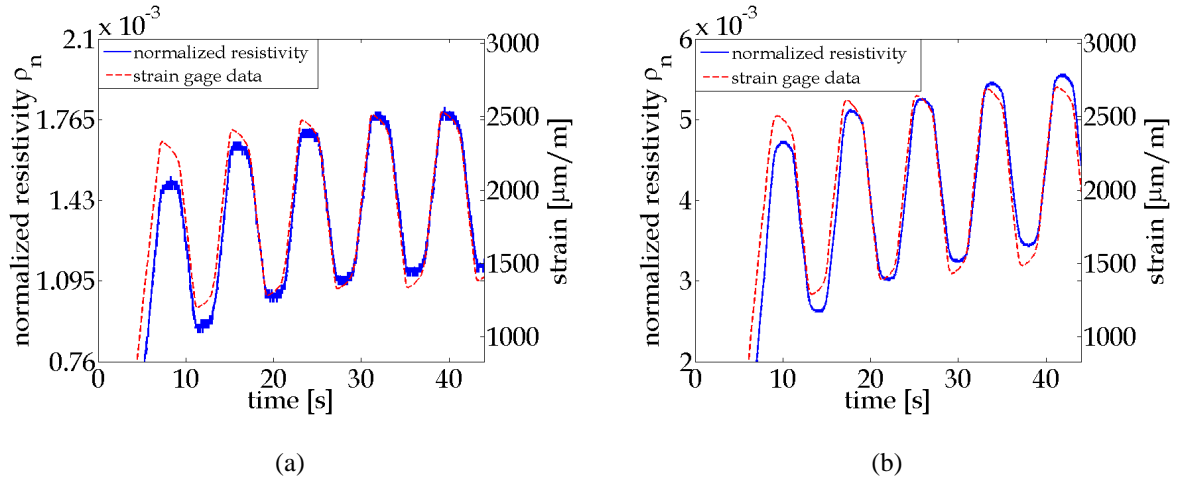


Figure 3.1 The normalized resistivity time history plots of PA 6 coupons coated with (a) MWNT-PSS and (b) MWNT-Pluronic thin films are overlaid with the applied strain time histories. The electrical properties of both thin films show good agreement with the applied strain profiles.

where ρ_0 is the initial resistivity of the thin film under unstrained condition. Figure 3.1 plots the applied strain profiles, and each plot was overlaid with the corresponding MWNT-PSS and MWNT-Pluronic thin film's normalized resistivity change. Similar to results presented in Mortenson *et al.* [17], the normalized resistivity behavior of the MWNT-PSS thin film showed good agreement with the cyclic strain pattern applied, and the strain-sensitive behavior remained consistent even after multiple loading cycles. The result in Figure 3.1(b) shows that the MWNT-Pluronic thin film exhibits similar resistivity response with respect to the applied strain pattern. Both thin films exhibited piezoresistivity. It can also be noticed that ρ_n from both thin films varied with different magnitudes in response to a similar range of applied strains/deformation; this result revealed differences in the intrinsic strain sensitivity of these materials, which will be discussed in the following paragraph.

The correlation between a thin film's resistivity variation and its strain variation quantifies the material's electrical sensitivity to mechanical deformation, or the strain sensitivity. In this study, the strain values of PA 6 coupons measured by strain gages are used to calculate their sprayed thin film's strain sensitivity. Figure 3.2 plots the normalized resistivity responses of both thin films as a function of the applied strains. A linear relationship between change in normalized resistivity and strain was found, and this result was consistent for both types of thin films; linearity over multiple cycles was also observed. Similar to any linear strain sensors, the thin film's strain sensitivity, S_e , can be expressed as:

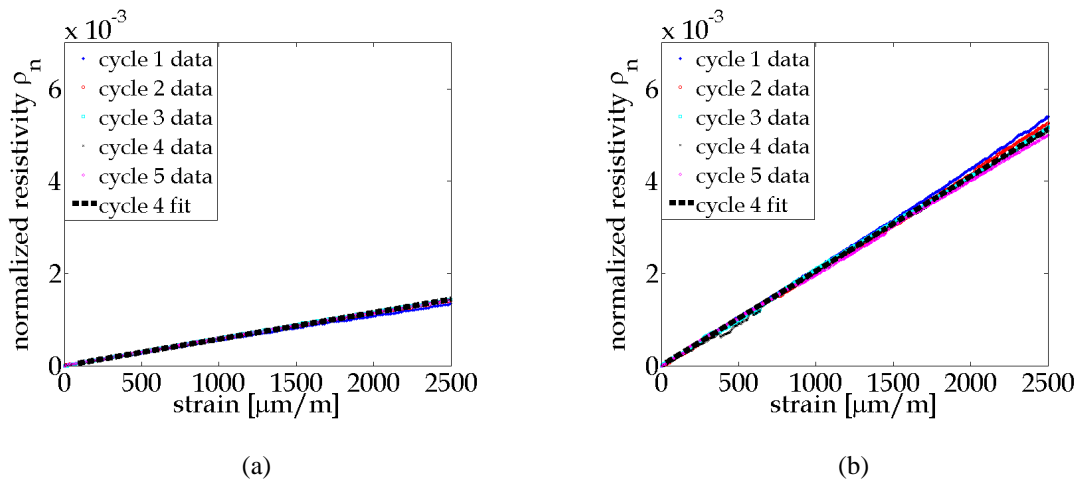


Figure 3.2 The (a) MWNT-PSS and (b) MWNT-Pluronic thin films' normalized change in resistivity with respect to the applied strains show their linear strain sensing properties.

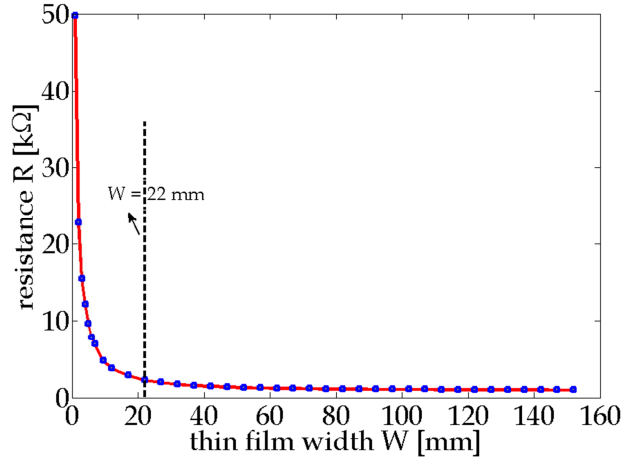


Figure 3.3 The gage resistance of an MWNT-PSS thin film was measured as the film's width was varied.

$$S_{\varepsilon} = \frac{\rho_n}{\varepsilon} \quad (3.2)$$

where ε is strain. A linear least-squares fit was applied to each loading cycle to calculate the thin film's strain sensitivity, and the final result presented is the average value of all the fittings from five load cycles applied to five different thin film specimens. Figure 3.2 shows examples of the linear fits (*i.e.*, the regression line fitted by using the data of cycle 4). The average value of the MWNT-PSS thin film's strain sensitivity (and standard deviation) was calculated to be 0.62 ± 0.12 ; this result was similar to the results reported by Mortenson *et al.* [17] (*i.e.*, 0.77 ± 0.02), as determined from tests conducted on freestanding MWNT-PSS thin films. The strain sensitivity of MWNT-Pluronic thin films is 2.06 ± 0.18 , similar to a foil-type strain gage. The result suggests that Pluronic as the polymeric stabilizer outperforms PSS in terms of improving the thin film's strain sensitivity by more than three times. Although its mechanism is still not completely understood, this improvement was thought to be due to a more stable, more uniform nanotube suspension. This result gives promise for enhancing the strain sensitivity of CNT-based thin films so that they can measure small strains.

3.2. Dimensional Influence over Thin Film's Electrical Response

Figure 3.3 plots the two-point probe resistance response versus the width of the thin film, whose gage length is 152 mm. The result shows that the thin film's gage resistance, R , was significantly influenced by its dimension when W is smaller than 22 mm; however, the response became relatively insensitive to the change of width when W becomes larger than 30 mm. This suggests that when a current passes through the thin film from one electrode to another, the effect of the thin film's dimension in the transverse direction becomes minor in responding to the electrical load. Figure 3.4 plots the absolute value of change in normalized resistivity $|\rho_n|$ with respect to the thin film's width-to-length ratio (W/L). The values of $|\rho_n|$ remain relatively constant until W/L exceeds 0.15, suggesting that the effective transverse range of electrical responses with respect to a perturbation along its gage length shall be within $W \leq 0.15L$. The result further suggests that the thin film would not be able to effectively respond to damage or strain deformation that take place outside the transverse range of $0.15L$ from its resistance measurement path (*i.e.*, at least if average resistance was measured using a two-point probe technique, which was done in this study).

4. CONCLUSIONS

In this study, an airbrushing technique used for fabricating carbon nanotube-polymer thin films was modified to create thin films with higher strain sensitivity. Pluronic replaced PSS as the carbon nanotube stabilizer to create an MWNT-suspension that was characterized by a prolonged shelf life, and it could be sprayed over any desired surface that was heated to an elevated temperature (55°C). The two-point probe resistance response of the MWNT-Pluronic thin film varied linearly in response to applied strain, and the strain sensitivity was found to be 2.06 ± 0.18 , which is more than three times higher than that of MWNT-PSS thin films fabricated using the same technique. In the second part of this study the effects of a thin film's width on its gage resistance were

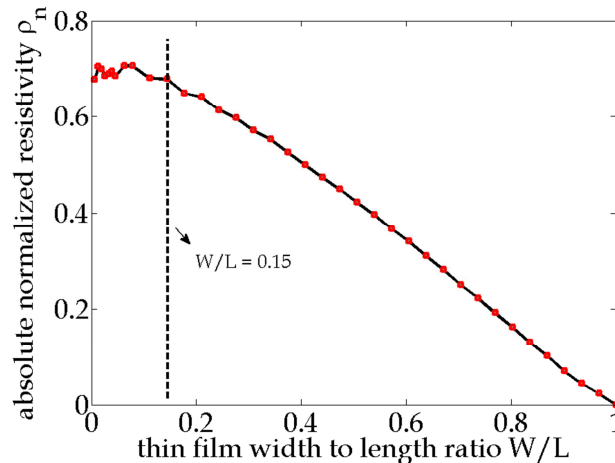


Figure 3.4 The absolute value of normalized resistivity of an MWNT-PSS film was plotted with respect to the width-to-length ratio.

investigated. The result showed that a two-point probe measurement of a thin film's resistance would not be able to pick up strain deformations or damages outside the $0.15L$ range in transverse direction to its gage length. Future research activities will be dedicated to applications of CNT-Pluronic thin films as two-dimensional spatial strain sensors over real-world FRP structures (*i.e.*, by coupling these films with an electrical impedance tomography algorithm).

ACKNOWLEDGEMENTS

The financial support by the Austrian Federal Ministry of Science, Research and Economy and the National Foundation for Research, Technology and Development is gratefully acknowledged. The authors would like to express their sincere appreciation to Professor Sabine Hild from the JKU Institute of Polymer Science for providing laboratory spaces and equipment for thin film fabrication. The JKU Institute of Biophysics was being extremely helpful for providing free access to their tip sonicator. Markus Grillenberger and Patrick Grüner are greatly appreciated for their assistance performing the research work. Professor Kenneth Loh is supported by the U.S. National Science Foundation (NSF) under grant no. CMMI-1200521.

REFERENCES

- Holbery, J. and Houston, D. (2006). Natural-Fiber-Reinforced Polymer Composites in Automotive Applications. *JOM*, **58:11**, 80-86.
- BMW Group. *The Future of Urban Mobility - BMW i*. (2015). Available from: www.bmw.com.
- Boeing. *787 Design Highlights - Advanced Composite Use*. (2015). Available from: www.boeing.com.
- Airbus. *A350 XWB - the Xtra That Makes the Difference*. (2015). Available from: www.airbus.com.
- Bakis, C., Bank, L.C., Brown, V., Cosenza, E., Davalos, J., Lesko, J., Machida, A., Rizkalla, S. and Triantafyllou, T. (2002). Fiber-Reinforced Polymer Composites for Construction-State-of-the-Art Review. *Journal of Composites for Construction*, **6:2**, 73-87.
- Ramakrishna, S., Mayer, J., Wintermantel, E. and Leong, K.W. (2001). Biomedical Applications of Polymer-Composite Materials: A Review. *Composites Science and Technology*, **61:9**, 1189-1224.
- Barré, S. and Benzeggagh, M.L. (1994). On the Use of Acoustic Emission to Investigate Damage Mechanisms in Glass-Fibre-Reinforced Polypropylene. *Composites Science and Technology*, **52:3**, 369-376.
- Berketis, K., Tzetzis, D. and Hogg, P. (2009). Impact Damage Detection and Degradation Monitoring of Wet GFRP Composites Using Noncontact Ultrasonics. *Polymer Composites*, **30:8**, 1043-1049.
- Schilling, P.J., Karedla, B.R., Tatiparthi, A.K., Verges, M.A. and Herrington, P.D. (2005). X-Ray Computed Microtomography of Internal Damage in Fiber Reinforced Polymer Matrix Composites. *Composites Science and Technology*, **65:14**, 2071-2078.
- Hofer, B. (1987). Fibre Optic Damage Detection in Composite Structures. *Composites*, **18:4**, 309-316.

11. Zhou, G. and Sim, L. (2002). Damage Detection and Assessment in Fibre-Reinforced Composite Structures with Embedded Fibre Optic Sensors-Review. *Smart Materials and Structures*, **11:6**, 925-939.
12. Loh, K.J. and Azhari, F. (2012). Recent Advances in Skin-Inspired Sensors Enabled by Nanotechnology. *JOM*, **64:7**, 793-801.
13. Lipomi, D.J., Vosgueritchian, M., Tee, B.C., Hellstrom, S.L., Lee, J.A., Fox, C.H. and Bao, Z. (2011). Skin-Like Pressure and Strain Sensors Based on Transparent Elastic Films of Carbon Nanotubes. *Nature nanotechnology*, **6:12**, 788-792.
14. Harris, P.J. (2009), Carbon Nanotube Science: Synthesis, Properties and Applications, Cambridge University Press.
15. Park, M., Kim, H. and Youngblood, J.P. (2008). Strain-Dependent Electrical Resistance of Multi-Walled Carbon Nanotube/Polymer Composite Films. *Nanotechnology*, **19:5**, 055705(7pp).
16. Li, Z., Dharap, P., Nagarajaiah, S., Barrera, E.V. and Kim, J. (2004). Carbon Nanotube Film Sensors. *Advanced Materials*, **16:7**, 640-643.
17. Mortensen, L.P., Ryu, D., Zhao, Y. and Loh, K.J. (2013). Rapid Assembly of Multifunctional Thin Film Sensors for Wind Turbine Blade Monitoring. *Key Engineering Materials*, **569-570**, 515-522.
18. Loh, K., Hou, T.-C., Lynch, J. and Kotov, N. (2009). Carbon Nanotube Sensing Skins for Spatial Strain and Impact Damage Identification. *Journal of Nondestructive Evaluation*, **28:1**, 9-25.
19. Loyola, B.R., Briggs, T.M., Arronche, L., Loh, K.J., La Saponara, V., O'Bryan, G. and Skinner, J.L. (2013). Detection of Spatially Distributed Damage in Fiber-Reinforced Polymer Composites. *Structural Health Monitoring*, **12:3**, 225-239.
20. Tallman, T., Gungor, S., Wang, K. and Bakis, C. (2014). Damage Detection and Conductivity Evolution in Carbon Nanofiber Epoxy via Electrical Impedance Tomography. *Smart Materials and Structures*, **23:4**, 045034(9pp).
21. Hou, T.-C. and Lynch, J.P. (2009). Electrical Impedance Tomographic Methods for Sensing Strain Fields and Crack Damage in Cementitious Structures. *Journal of Intelligent Material Systems and Structures*, **20:11**, 1363-1379.
22. Loyola, B.R. (2012). Distributed *in-situ* Health Monitoring of Conductive Self-Sensing Fiber-Reinforced Polymers Using Electrical Impedance Tomography, Ph.D. Thesis in *Mechanical and Aerospace Engineering*. University of California, Davis, Davis, CA, USA.
23. Voge, C.M., Johns, J., Raghavan, M., Morris, M.D. and Stegemann, J.P. (2013). Wrapping and Dispersion of Multiwalled Carbon Nanotubes Improves Electrical Conductivity of Protein-Nanotube Composite Biomaterials. *Journal of Biomedical Materials Research Part A*, **101:1**, 231-238.
24. Shvartzman-Cohen, R., Florent, M., Goldfarb, D., Szeifer, I. and Yerushalmi-Rozen, R. (2008). Aggregation and Self-Assembly of Amphiphilic Block Copolymers in Aqueous Dispersions of Carbon Nanotubes. *Langmuir*, **24:9**, 4625-4632.
25. Chen, S.-H., Liao, C., Fratini, E., Baglioni, P. and Mallamace, F. (2001). Interaction, Critical, Percolation and Kinetic Glass Transitions in Pluronic L-64 Micellar Solutions. *Colloids and Surfaces A: Physicochemical and Engineering Aspects*, **183-185**, 95-111.